Observed Land Impacts on Clouds, Water Vapor, and Rainfall at Continental Scales

MENGLIN JIN,[1] AND MICHAEL D. KING[2]

Short title: Land Impacts At Continental Scales

Quarterly Journal of the Royal Meteorological Society
(Manuscript submitted March 2005)

[1] Department of Meteorology, University of Maryland, College Park, Maryland.
[2] Earth-Sun Exploration Division, NASA Goddard Space Flight Center, Greenbelt, Maryland.

SUMMARY

How do the continents affect large-scale hydrological cycles? How important can one continent be to the climate system? To address these questions, 4-years of National Aeronautics and Space Administration (NASA) Terra Moderate Resolution Imaging Spectroradiometer (MODIS) observations, Tropical Rainfall Measuring Mission (TRMM) observations, and the Global Precipitation Climatology Project (GPCP) global precipitation analysis, were used to assess the land impacts on clouds, rainfall, and water vapor at continental scales. At these scales, the observations illustrate that continents are integrated regions that enhance the seasonality of atmospheric and surface hydrological parameters. Specifically, the continents of Eurasia and North America enhance the seasonality of cloud optical thickness, cirrus fraction, rainfall, and water vapor. Over land, both liquid water and ice cloud effective radii are smaller than over oceans primarily because land has more aerosol particles. In addition, different continents have similar impacts on hydrological variables in terms of seasonality, but differ in magnitude. For example, in winter, North America and Eurasia increase cloud optical thickness to 17.5 and 16, respectively, while in summer, Eurasia has much smaller cloud optical thicknesses than North America. Such different land impacts are determined by each continent's geographical condition, land cover, and land use. These new understandings help further address the land-ocean contrasts on global climate, help validate global climate model simulated land-atmosphere interactions, and help interpret climate change over land.

1. INTRODUCTION

Land is known to have a larger global warming signal [*NRC*, 2000; *Jin and Dickinson*, 2002; *Jin*, 2004] than oceans, suggesting that the former affects and responds to the global climate system differently than the latter. With use of recently available satellite observations, this study examines the land impacts on clouds, water vapor, and rainfall, with a focus on the continental scale.

Studying land impacts at continental scales is essential, since land-ocean contrasts on surface temperature determines surface circulation (Rasmusson *et al.* 1993), which in turn modifies the atmospheric 3-cell circulation and consequently affects the displacement of large-scale clouds and rainfall systems (Bjerknes 1966; Wallace and Patton 1970; Holton 2004; Wallace and Hobbs 1977; Lau 1982). Most studies of land impacts on climate have been at local (e.g., urban) or regional (e.g., deforestation) scales. How land differs from ocean on continental scales is an important question that needs to be addressed in order to fully understand land-atmosphere interaction. For example, land use and land cover prove to be one of the dominant forces for local and regional climate change (Henderson-Sellers *et al.* 1988; Shuttleworth *et al.* 1991; Sud et al. 1996; Jin and Zhang 2002). Studies show that urbanization modifies nearby rainfall intensity, duration, and peak time (Shepherd and Burian 2003; Shepherd 2004) and changes surface temperature, aerosol, and cloud features [Landsberg 1970; Oke 1982; Jin *et al.* 2005a,b). Nevertheless, the integrated impacts of land as a continent, which should more significantly affect global energy and water cycles, are understudied. Finally, observed continental impacts can be used to validate whether general circulation models (GCMs), such as those used in the National Centers for Environmental Prediction (NCEP) and European Centre for Medium-Range Weather Forecasts (ECMWF), can reproduce such features. In GCM evaluations, two approaches are generally accepted to fuse satellite observations in GCMs.

One is to optimize the model parameters based on satellite observations (Jin and Liang 2005). Another is to analyze observations to advance the understanding of certain physical processes, and then improve the capability of simulating such processes (Jin and Shepherd 2005). The National Aeronautics and Space Administration (NASA) Terra Moderate Resolution Imaging Spectroradiometer (MODIS) observations provide rich information that is useful to improve our understanding of land-atmosphere interactions.

Clouds, water vapor, and rainfall are closely related to each other. To study land continental impacts on the hydrological cycle, these three variables need to be examined simultaneously. Covering about 70% of the Earth's surface, clouds reflect shortwave radiation and absorb and emit longwave radiation. Therefore, their importance in the Earth's climate system cannot be overestimated (Arakawa 2004). ISCCP data for 1982-1996 showed that 64% of the globe is covered by clouds, while only 54% of the Northern Hemisphere land, 53% of the Southern Hemisphere land, 66% of the Northern Hemisphere ocean, and 70% of the Southern Hemisphere ocean is covered by clouds. A slight difference in daytime and nighttime was also detected (Hahn *et al.* 1994) (www.agci.org/publications/eoc94/EOC1/EOC1-25.html). With the advent of the multispectral and high spatial resolution MODIS instrument on Terra and Aqua, these newer observations show that the globe is generally 68-70% covered by clouds, depending on satellite. Unfortunately, clouds are the major uncertainty in model response to climate forcing (Cess *et al.* 1989). Accurate measurements on cloud properties including cloud optical thickness, cloud particle size, cloud cover, and cloud spatial, vertical, and temporal distribution are highly desired.

Water vapor is the most abundant greenhouse gases in the atmosphere (IPCC 2001). Thus, water vapor links closely with temperature, as increases of

water vapor correspond to surface and atmospheric warming in forms of latent heat release in water phase change (Chahine 1992). The global distribution of total column atmosphere water vapor is determined by surface temperature, with the peak typically over equatorial regions and the minimum over cold Polar Regions. In general, the tropical regions contain 6 cm of water vapor, 10 times more than that of Polar Regions (Randel *et al.* 1996). The most humid region of the globe is the west equatorial Pacific Ocean, where so-called "warm pool" sea surface temperatures make the atmospheric temperature high and thus able to hold more moisture. Equatorial desert regions have regional minima in part because the deserts are extremely dry due to subsidence. The vertical distribution of water vapor is also well known, decreasing rapidly from the surface to higher altitudes with about 50% below 850 hPa (IPCC 2001, chapter 7). The global average turn over time for water vapor is 9 days (Seidel 2002), given the fact that the global average precipitable water is ~2.5 cm if it rains to the surface, but the annual global precipitation is ~1 m.

This paper makes extensive use of MODIS observations, combined with the Tropical Rainfall Measuring Mission (TRMM) and Global Precipitation Climatology Project (GPCP) global precipitation analysis, to examine monthly cloud, water vapor, and rainfall seasonal and interannual variations for eventually a better understanding of land continental impacts on atmospheric hydrological variables. In particular, we will address the following questions:

(a) What are the observed geographical distributions of water vapor, rainfall, cirrus fraction, cloud optical thickness, effective cloud liquid droplet size, and effective ice particle size?

(b) What are the continental average values for these variables over given regions and seasons? What are the maxima and minima of these variables on continental averages?

The next section (Section 2) describes data sets and background information on water vapor, clouds, cirrus, and rainfall retrieval. Section 3 discusses results, and is followed by a section of final discussion and remarks (Section 4).

2. DATA

More than three years (April 2000 to July 2003) of cloud properties, including cloud optical thickness[3], cirrus fraction, water vapor, and effective radius for water and ice clouds measured by MODIS (Gao *et al.* 2002; King *et al.* 2003; Platnick *et al.* 2003; Seeman *et al.* 2004) were used in this study. MODIS uses infrared bands to determine cloud physical properties related to cloud top pressure and temperature, and visible and near-infrared bands to determine cloud optical and microphysical properties. Nakajima and King (1990) showed that the reflection function of clouds at a non-absorbing band in the visible wavelength region (e.g., 0.66 μm) is primarily a function of cloud optical thickness, whereas the reflection function at a water (or ice) absorbing channel in the near-infrared (i.e., 1.6 or 2.1 μm) is a function of cloud particle size. This algorithm, together with extensions to distinguish between liquid water and ice clouds and to consider reflection by various underlying surfaces, including snow and sea ice (King *et al.* 2004), has been incorporated into the operational MODIS retrieval algorithm. MODIS gives cloud droplet size (r_e) in two thermodynamic phases, viz., cloud effective droplet size for liquid water (r_{ew}) and for ice (r_{ei}). The cloud liquid (and ice) water path is calculated from the retrieved cloud optical thickness (τ_c) and effective radius

---

[3] Cloud optical thickness is a dimensionless integral of the extinction coefficient along a vertical path through the cloud. It is determined by liquid water path and effective radius. Liquid water path is the weight of liquid water droplets in the atmosphere above a unit surface area on the earth {g m^{-2}}. Effective radius is the ratio of volume to area of cloud drops, droplets, or ice crystals integrated over the cloud particle size distribution.

r_e.

The MODIS-derived atmospheric profiles product (King *et al.* 2003; Seemann *et al.* 2003) is produced using 12 infrared bands with wavelengths between 4.47 and 14.24 μm, and includes atmospheric profiles of atmospheric temperature and moisture layers, total column ozone, and total precipitable water. Of particular interest to this study is the water vapor in the total atmospheric column, which has important applications to climate studies.

Corresponding monthly mean rainfall measurements from NASA TRMM (Simpson *et al.* 1988) and GPCP microwave and geosynchronous satellite analysis (Adler *et al.* 2003) are used to show the different features of surface precipitation over different continents. Specifically, we analyzed land rain gauge data originally provided by Global Precipitation Climatology Center (GPCC). The spatial resolution of the data is 1° x 1° for TRMM and 2.5° x 2.5° for GPCP.

3. RESULTS

Cloud optical thickness (τ_c) varies across the globe and has evident seasonality (Figure 1). The optically thickest clouds are present over land rather than over the ocean, in particular over west Eurasia, east Asia, and southeastern South America. The cloud optical thicknesses over these areas are about 30 all year around. The minimum τ_c (< 10) occurs over ocean regions related to subtropical subsidence. In addition, other regions, including eastern North America and Greenland have large τ_c up to 30 during winter months (cf. November–January). No satellite observations are available for Greenland during winter months because the satellite algorithm requires reflected sunlight, but large τ_c values are observed in September, October, and February.

Globally averaged cloud optical thickness over land is larger than that of ocean, with values ranging from 12-15 for land but only 11-12 for ocean (Figure

2a). Larger τ_c corresponds to more reflection or scattering to shortwave downward solar radiation, and results in less surface insolation. In addition, land has more evident seasonality than ocean does. The peak τ_c of land occurs in October 2000-2002 and in November 2003. Continental-wide averaged τ_c for North America, Eurasia, and the whole Northern Hemisphere (poleward of 70°N is not included) is shown in Figure 2b, further proving that land has larger τ_c than ocean. Furthermore, each continent has distinct seasonality. For example, North America has higher τ_c than Eurasia. Both Eurasia and North America have peak τ_c during winter seasons (November-February), while North America has its minimum τ_c in March and Eurasia has its minimum in July or August. Finally, Eurasia has relatively noisier seasonal and interannual variations than North America.

Clouds result from large-scale dynamics as well as local convection. Therefore, analyses over different regions serve to illustrate what region, with corresponding dynamical or thermodynamical systems, contributes most to the continentally-averaged seasonality observed in Figure 2. Figure 3 shows that zonally-averaged τ_c over 0°-10°N and 30°-40°N have the largest differences among land and ocean surfaces. For all 10° latitude zones (e.g., 0°-10°N, 10°-20°N, 20°-30°N, 40°-50°N, and 50°-60°N), land τ_c are larger than the cloud optical thickness of ocean regions. Although all zonal bands have distinct seasonality, they are different in many details. First, the amplitude of seasonality (peaks minus minimum values) is different. The smallest seasonality occurs in 20°-30°N and the largest seasonality in 50°-60°N. Second, low latitudes (0°-10°N, 10°-20°N) have peak values of τ_c in July and minimum values during January-March, but high latitudes (40°-50°N, 50°-60°N) have peak τ_c occurring in January. In addition, high latitudes have much larger τ_c than low latitudes do. For example, 50°-60°N has the minimum τ_c of 14 and a maximum τ_c of 15 in January. Over the North-

ern Hemisphere, the lowest zonal τ_c occurs in 10°-20°N during the wintertime, with a value only 5.5 for both land and ocean in January 2001, March 2002 and March 2003.

Figure 4 shows the geographical distributions of cloud effective radius for water clouds (r_{ew}) and ice clouds (r_{ei}), averaged from April 2000 to July 2004. The overall pattern between r_{ew} (Figure 4a) and τ_c are very similar. For liquid water clouds, the maximum cloudlet size occurs over western tropical Pacific warm pool region, where large evaporation associated with large sea surface temperature exists. Both land and ocean have large r_{ew} variations with the minimum as low as 5 and the maximum monthly mean up to ~22 μm in the tropical ocean regions. In general, oceans have larger values of r_{ew} and relatively moderate variations, whereas land surfaces have smaller values of r_{ew} because land regions have more aerosols that serve as cloud condensation nuclei (CCN).

In contrast, for ice clouds, the particle size has relatively small differences between land and ocean, except over snow and sea ice surfaces such as the Antarctic continent and high northern latitudes (Figure 4b). A closer look on the continental scale (Figure 5) further confirms that land has smaller r_e than ocean, especially for liquid water clouds, and has larger seasonal variations for both liquid water and ice clouds. Specifically, r_{ew} varies from 11 to 14.5 μm for the North American continent (13 to 14.5 μm for Eurasia) but much more moderately for the Northern Hemisphere that includes both land and ocean from 13.5 to 15.2 μm (Figure 5b). Furthermore, North America has a larger interannual r_{ew} variation than Eurasia. By comparison, the differences in r_{ei} between the three regions are much less distinct, with r_{ei} being the largest in January and February and the smallest in July, in stark contrast to r_{ew}, which is largest in July and the smallest in January and February. In addition, r_{ei} ranges from 25-29 μm continentally (Figure 5a), which is larger than the hemisphere average, suggesting that land

increases the spread of r_{ei}.

Similar to τ_c, cirrus fraction varies across the globe and has evident seasonality (Figure 6), with maximum occurring over the Tibetan plateau region. Low values are observed over subtropical subsidence and North Pole regions where low humidity and low temperature are present. A maximum of ~0.8 occurs over the Antarctic continent in the Spring and Summer months (September–February), and Greenland and North America in March and April related to the transition time. The Andes has high cirrus fraction all year around. In general, land has higher cirrus fraction than ocean. For example, Asia has a cirrus fraction around 0.5 in all months, while most ocean regions have <0.3 in the tropics and subtropics.

At continental scales, land enhances the amplitude of the annual cycle of cirrus fraction by about 50% (Figure 7), since the Northern Hemisphere ranges from 0.35-0.45, but North America ranges from 0.35-0.60 and Eurasia from 0.27-0.5. Specifically, the seasonality of cirrus fraction is clear for both continents with minima in July and August and maxima in March.

Globally, land has persistently lower water vapor amounts than ocean regions (Figure 8a). Water vapor ranges from 11.5 to 13 cm [Menglin – the units in Figure 8 and in the text here don't make sense; the global water vapor ranges from <0.5 to ~ 5 cm as shown in Figure 9, with a global mean of around 2.5-3 cm] for global ocean and from 10.8 to 12.8 for global land. This may be because oceans have adequate supplies of liquid water at the surface and thus should have maximum evaporation. Nevertheless, water vapor here is column integrated precipitable water, which is determined by surface as well as atmosphere temperatures, dynamics, and surface sources of water (Randel *et al.* 1996). In addition, continents can differ from each other in their water vapor content (Fig. 8b). Eurasia has higher water vapor than North America by up to 40% in Janu-

ary 2002, with 18 cm for Eurasia and 13 cm for North America. In July, both continents hold more water vapor than they do in January. The different relationship of land and ocean water vapor between Figures 8a and 8b, namely, globally land has less water vapor than oceans but for specific continents (Eurasia and North America) land has much larger amounts of water vapor than the global mean ocean. This suggests that other continents may be much drier and thus reduce the land-averaged water vapor column amount.

To examine all continents, Figure 9a shows the MODIS-derived global distribution of column water vapor, which varies dramatically over land and ocean. In general, because water vapor is a function of surface temperature, zonal decreases from the moist tropics to the drier Polar Regions are evident. Equatorial regions have higher water vapor because of high surface temperature and adequate water supplies from of water from the surface. Greenland, the Tibetan plateau, and the Andes Mountains have minimum water vapor because of low temperature in the atmosphere that can thus hold little water vapor. The Saharan Desert and neighboring Arabian Peninsula have small water vapor content because little water can be transported and held in these hot desert regions. Evident seasonal changes of water vapor over the globe are observed in Figures 9a and 9b. In January, land over the Northern Hemisphere has uniformly smaller water vapor (less than 0.5 cm) because of the cold land and atmospheric temperature at that time of year. In addition, the maximum centers of water vapor have shifted south in January, which is related to the seasonal variation of solar illumination.

A study of land impact on the atmospheric hydrological cycle would not be complete without examining rainfall, as water vapor, clouds, and rainfall are closely related to one other. Figure 10 shows two monthly mean rainfall accumulation images for January and July, respectively. Ocean regions generally

have larger rainfall than land regions in tropical and subtropical areas, but such differences are further complicated by land cover evapotranspiration. For example, Amazonian forests have significantly more accumulated rainfall than nearby oceans because of the strong evapotranspiration and local convective activity (ref).

As was the case for water vapor and clouds, evident seasonal variation of rainfall can be observed for certain regions (Fig. 10b). Further analysis of zonally-averaged monthly rainfall accumulation from TRMM (Figure 11) shows that 5°N has its maximum rainfall amount in July of up to ~220 mm, and such maxima shift to 5°S in January and reduces to ~160 mm. Minimum rainfall occurs from 10°-20°N and 10°-20°S, related to subtropical subsidence, where the monthly mean rainfall is generally <20 mm.

At continental scales, seasonality of rainfall is significant (Figure 12). In July, both Eurasia and North America have much larger rainfall than they do in January. Nevertheless, North America seems to have its peak in September instead of July as in Eurasia. In addition, both continents differ from each other in terms of absolute values of accumulated rainfall. For example, in January 2001, North America had 40 mm of rainfall while Eurasia had only 20 mm, a 50% decrease in continental average. Such differences must be related to both large-scale dynamics as well as local land cover mechanisms (Jin and Zhang 2002). Note that rainfall for the Northern Hemisphere in Figure 12 is based on GPCP rain gauge station data and is only over land and islands. Therefore, the ocean effects cannot directly be included in this figure. Nevertheless, this figure examines the seasonal variation of rainfall for land surfaces and suggests interrelationship between rainfall, clouds, and water vapor.

4. DISCUSSIONS AND REMARKS

This paper provides a prototype application of using MODIS and other observations to better understand land-atmosphere interactions. Analyses of the land impacts on clouds, water vapor, cirrus fraction, and rainfall at continental scales from 2000 to 2004 illustrate that land enhances the seasonality of these variables, namely, land enhances the seasonal variation of cloud optical and microphysical properties, column water vapor, and rainfall. Furthermore, land decreases the cloud effective radius, especially for liquid water clouds. Different continents have different characteristics, which in turn are related to details of their land cover, geographic location, and nearby oceanic circulation.

Scale is important in studying land impacts and climate change. Global scales and continental scales may have different distinguishing features. For example, the Eurasian and North American continents hold more precipitable water (column water vapor) than oceans in summer because land areas are warmer than the nearby oceans, but in the global mean, the atmosphere over the land has less water vapor than over oceans in large part because land over high latitudes is much colder and hence contains much less water vapor.

Cloud simulation is one of the weakest parts of the current GCMs, partly because of the lack of accurate knowledge of cloud dynamics, cloud microphysics, cloud-aerosol interactions, and partly because of the unrealistic specification on sub-grid cloud features. For example, the NCAR GCM, like many other GCMs, prescribes cloud effective radius of liquid water as 10 μm over oceans and 7-10 μm over land, while MODIS observations show obviously spatial and temporal variations with a maximum up to 20 μm for liquid droplets over tropical ocean (cf. Figure 4). Over land, r_{ew} and r_{ei} vary with the underlying surface and aerosol properties through cloud-aerosol interactions (cf. Figure 5). Since in the model r_e is used to calculate other cloud radiative properties (namely, cloud opti-

cal depth, single scattering albedo, asymmetry factor, and cloud effective emissivity), any error in the prescribed r_e may propagate into the model's cloud properties and may further propagate into surface temperature and rainfall simulations. Therefore, realistic cloud droplet size is very important in model cloud parameterization.

Accurate cloud, water vapor, and rainfall simulations in climate models require knowledge of land-atmosphere interactions, the basic feature that determines the global water and energy transport. Current GCMs needs observations to validate and improve the models. For example, Figure 13 shows the NCEP reanalysis simulated column water vapor, which is evidently different from MODIS observations (cf. Figure 8b) in both the relative pattern and in quantitative values. MODIS shows the peaks of water vapor occurring in January for Eurasia and North America, but NCEP shows a minimum then [Menglin – again I think Figure 8 does not look reasonable, and think that the NCEP result is more consistent with Figure 9; please check Figure 8 carefully]. In addition, MODIS shows land increases the peaks and decreases the minima, but NCEP shows land and ocean having similar peak time and values. This example suggests the importance of using satellite observations to validate and improve GCMs for a possibly better simulation of the climate system.

Unfortunately, a clear gap exists between remote sensing observations and climate model requirements, partly because limited resources hinder an in depth analysis of the rich information content that MODIS, TRMM, and other observations contain, and partly because of the mismatch in the remote sensing and modeling communities. One example for the latter is resolution—MODIS can give 1 km spatial resolution observations while model grid are typically about 100 km. How to scale up high-resolution data meaningfully for GCM use is a challenging task. Only a collaboration between remote sensing experts and

modelers can possibly fill the gap and make more effective use of satellite observations into GCMs.

Although remote sensing data by themselves are extremely valuable, their uncertainty requires special attention in using these data in climate studies or for improving GCMs. Like any other measurements, MODIS observations have reported uncertainties, for example, instantaneous errors of column water vapor over a 1.5 year time period are accurate to an rms error of about 4.1 mm when compared to collocated ground-based microwave radiometer observations (Seemann *et al.* 2003), and ice effective radius is accurate to about 1.5 μm for optically thin cirrus clouds when compared to collocated ground-based millimeter cloud radar observations (Mace *et al.* 2005). It is important for the users to realize that using data to study the patterns and differences, namely, seasonal, diurnal and interannual variations, rather than absolute values, shall make the final result less affected by the uncertainty of the observations.

ACKNOWLEDGMENTS

We thank NASA EOS Interdisciplinary Science and TRMM programs for supporting this work. Special thanks go to Dr. Zhong Liu of NASA DAAC for his extremely helpful on-line data analysis and visualization tools for MODIS and TRMM data. NCEP reanalysis data were downloaded from the NOAA-CIRES Climate Diagnostics Center (www.cdc.noaa.gov/cdc/reanalysis/reanalysis.shtml).

REFERENCES

Adler, R. F., Huffman, G. J., Chang, A., Ferraro, R., Xie, P. P., Janowiak, J., Rudolf, B., Schneider, U., Curtis, S., Bolvin, D., Gruber, A., Susskind, J., Arkin, P. and Nelkin E. 2003 The version 2 Global Precipitation Climatology Project (GPCP) monthly precipitation analysis (1979 present). *J. Hydrometeor.*, **4**, 1147-1167

Arakawa, A. 2004 The cumulus parameterization problem: Past, present, and future. *J. Climate*, **17**, 2493-2525

Bjerknes, J. 1966 A possible response of atmospheric Hadley circulation to equatorial anomalies of ocean temperature. *Tellus*, **18**, 820-829

Cess, R. D., Potter, G. L., Blanchet, J. P., Boer, G., Ghan, S. J., Kiehl, J. T., Liang, X. Z., Mitchell, J. F. B., Morcrette, J. J., Randall, D. A., Riches, M. R., Roeckner, E., Schlese, U., Slingo, A., Taylor, K. E., Washington, W. M., Wetherald, R. T. and Yagai, I. 1989 Intercomparison and interpretation of cloud-climate feedback as produced by fourteen atmospheric general circulation models. *Science*, **245**, 513-516

Chahine, M. T. 1992 The hydrological cycle and its influence on climate. *Nature*, **359**, 373-380

Gao, B. C., Yang, P., Han, W., Li, R. R. and Wiscombe, W. J. 2002 An algorithm using visible and 1.38-μm channels to retrieve cirrus cloud reflectances from aircraft and satellite data,, *IEEE Trans. Geosci. Remote Sens.*, **40**, 1659-1668

Hahn, C. J., Warren, S. G. and London, J. 1994 *Edited Synoptic Cloud Reports from Ships and Land Stations Over the Globe, 1982-1991*. NDP-026B, Carbon Dioxide Information Analysis Center, Oak Ridge National Laboratory, Oak Ridge, Tennessee

Henderson-Sellers, A., Dickinson, R. E., and Wilson, M. F. 1988 Tropical deforestation—Important processes for climate models. *Climate Change*, **13**, 43-67

Holton, J. R. 2004 *Introduction to Dynamic Meteorology,*

Fourth Edition. Elsevier Academic Press, 529 pp.

IPCC, The Intergovernmental Panel on Climate Change 2001 *Climate Change 2001: The Scientific Basis.* Cambridge University Press, 881 pp.

Jin, M. 2004 Analyzing skin temperature variations from long-term AVHRR. *Bull. Amer. Meteor. Soc.*, **85,** 587-600

Jin, M. and Dickinson, R. E. 2002 New observational evidence for global warming from satellite data. *Geophys. Res. Lett.*, **29***(10)*, doi:10.1029/2001GL013833

Jin, M. and Zhang D. L. 2002 Changes and interactions between skin temperature and leaf area index in summer 1981-1998. *Meteor. Atmos. Phys.*, **80,** 117-129

Jin, M. and Shepherd, J. M. 2005 On including urban landscape in land surface models—How can satellite data help? *Bull. Amer. Meteor. Soc.*, **86,** in press

Jin, M. and Liang, S. 2005 Improving land surface emissivity parameter of land surface model in GCM. *J. Climate,* in press

Jin, M., Dickinson, R. E. and Zhang, D. L. 2005a The footprint of urban areas on global climate as characterized by MODIS. *J. Climate,* **18,** in press

Jin, M., Shepherd J. M. and King, M. D. 2005b Urban aerosols and their interaction with clouds and rainfall: A case study for New York and Houston. *J. Geophys. Res.*, in press

King, M. D., Menzel, W. P., Kaufman, Y. J., Tanré, D., Gao, B. C., Platnick, S., Ackerman, S. A., Remer, L. A., Pincus, R. and Hubanks, P. A. 2003 Cloud and aerosol properties, precipitable water, and profiles of temperature and humidity from MODIS. *IEEE Trans. Geosci. Remote Sens.*, **41,** 442-458

King, M. D., Platnick, S., Yang, P., Arnold, G. T., Gray, M. A., Riédi, J. C., Ackerman, S. A. and Liou, K. N. 2004 Remote sensing of liquid water and ice cloud optical thickness and effective radius in the arctic: Application of airborne multispectral MAS data. *J. Atmos. Oceanic Technol.*, **21,** 857-875

Landsberg, H. E 1970 Man-made climatic changes *Science,* **170,** 1265-1274

Lau, K. M 1982 Thermally driven motions in an equatorial beta-plane: Hadley and Walker circulations during the winter mon-

soon. *Monthly Weather Review*, **110**, 336-353

Mace, G. G., Zhang, Y., Platnick, S., King, M. D., Minnis, P. and Yang, P. 2005 Evaluation of cirrus cloud properties derived from MODIS data using cloud properties derived from ground-based observations collected at the ARM SGP site. *J. Appl. Meteor.*, in press

Martin, G. M., Johnson, D. W. and Spice, A. 1994 The measurement and parameterization of effective radius of droplets in warm stratocumulus clouds. *J. Atmos Sci.*, **51**, 1823-1842

Nakajima, T. and King, M. D. 1990 Determination of the optical thickness and effective particle radius of clouds from reflected solar radiation measurements. Part I: Theory. *J. Atmos. Sci.*, **47**, 1878-1893

National Research Council (NRC 2000 Reconciling observations of global temperature change. *National Academy Press*

Oke, T. R. 1982 The energetic basis of the urban heat island. *Quart. J. Roy. Meteor. Soc.*, **108**, 1-24

Platnick, S., King, M. D., Ackerman, S. A., Menzel, W. P., Baum, B. A., Riédi, J. C. and Frey, R. A. 2003 The MODIS cloud products: Algorithms and examples from Terra, *IEEE Trans. Geosci. Remote Sens.*, **41**, 459-473

Randel, D. L., Vonder Haar, T. H., Ringerud, M. A., Stephens, G. L., Greenwald, T. J. and Combs, C. L. 1996 A new global water vapor data set. *Bull. Amer. Meteor. Soc.*, **77**, 1233-1246

Rasmusson, E. M., Dickinson, R. E., Kutzbach, J. E., and M. K. Cleveland 1993 Climatology. *Handbook of Hydrology*, D. R. Maidment, Ed., McGraw-Hill Professional, 2.1-2.43

Seemann, S. W., Li, J., Menzel, W. P. and Gumley, L. E. 2003 Operational retrieval of atmospheric temperature, moisture, and ozone from MODIS infrared radiances. *J. Appl. Meteor.*, **42**, 1072-1091

Seidel, D. J. 2002 Water vapor: Distribution and trends. *Encyclopedia of Global Environmental Change*, John Wiley & Sons, Ltd.

Shepherd, J. M. and Burian, S. J. 2003 Detection of urban-induced rainfall anomalies in a major coastal city. *Earth Interactions*, **7(4)**, doi:

10.1175/10873562 (2003)007

Shepherd, J. M., Pierce, H. and Negri, A. J. 2002 Rainfall modification by major urban areas: Observations from spaceborne rain radar on the TRMM satellite *J. Appl. Meteor.*, **41**, 689-701

Shuttleworth, W. J., J. H. C. Gash, J. M. Roberts, C. A. Nobre, L. C. B. Molion, and M. N. G. Ribeiro 1991 Post-deforestation Amazonian climate: Anglo-Brazilian research to improve prediction. *J. Hydrol.*, **129**, 71-85

Sud, Y. C., Walker, G. K., Kim, J. H., Liston, G., Sellers, P. J. and Lau, W. K. M. 1996 Biogeophysical consequences of a tropical deforestation scenario: AGCM simulation study. *J. Climate*, **9**, 3225-3247

Simpson, J., Adler, R. F. and North, G. R. 1988 A proposed Tropical Rainfall Measuring Mission (TRMM) satellite. *Bull. Amer. Meteor. Soc.*, **69**, 278-295

Twomey, S. 1977 The influence of pollution on the shortwave albedo of clouds. *J. Atmos. Sci.*, **34**, 1149-1152

Wallace, J. M. and Hobbs, P. V. 1977 *Atmospheric Sciences: An Introductory Survey*. Academic Press, Inc., 467 pp.

Wallace, J. M. and Patton, D. B. 1970 Diurnal temperature variations—Surface to 25 kilometers. *Mon. Wea. Rev.*, **98**, 548-552

FIGURE LEGENDS

Figure 1. Monthly mean cloud optical thickness from April 2000-July 2003.

Figure 2. Monthly mean cloud optical thickness as a function of time (a) for global land and ocean, and (b) for North America, Eurasia, and the Northern Hemisphere.

Figure 3. Zonal mean cloud optical thickness as a function of time for land and ocean regimes.

Figure 4. Monthly mean cloud effective radius for (a) liquid water clouds and (b) ice clouds from April 2000-July 2003.

Figure 5. Monthly mean cloud effective radius as a function of time for (a) ice clouds and (b) liquid water clouds.

Figure 6. Monthly mean cirrus fraction from April 2000-July 2003.

Figure 7. Monthly mean cirrus fraction as a function of time for North America, Eurasia, and the Northern Hemisphere.

Figure 8. Monthly mean precipitable water as a function of time (a) for global land and ocean, and (b) for North America, Eurasia, and the Northern Hemisphere ocean.

Figure 9. Monthly mean precipitable water for (a) July 2004 and (b) January 2004.

Figure 10. Accumulated rainfall measured from TRMM for (a) July 2003 and (b) January 2004.

Figure 11. Zonally-averaged monthly mean accumulated rainfall from TRMM observations at 180°W.

Figure 12. Monthly rainfall for the Northern Hemisphere, North America, and Eurasia. Data are based on GPCP analysis.

Figure 13. NCEP reanalysis simulated precipitable water vapor for North America, Eurasia, and the North Hemisphere.

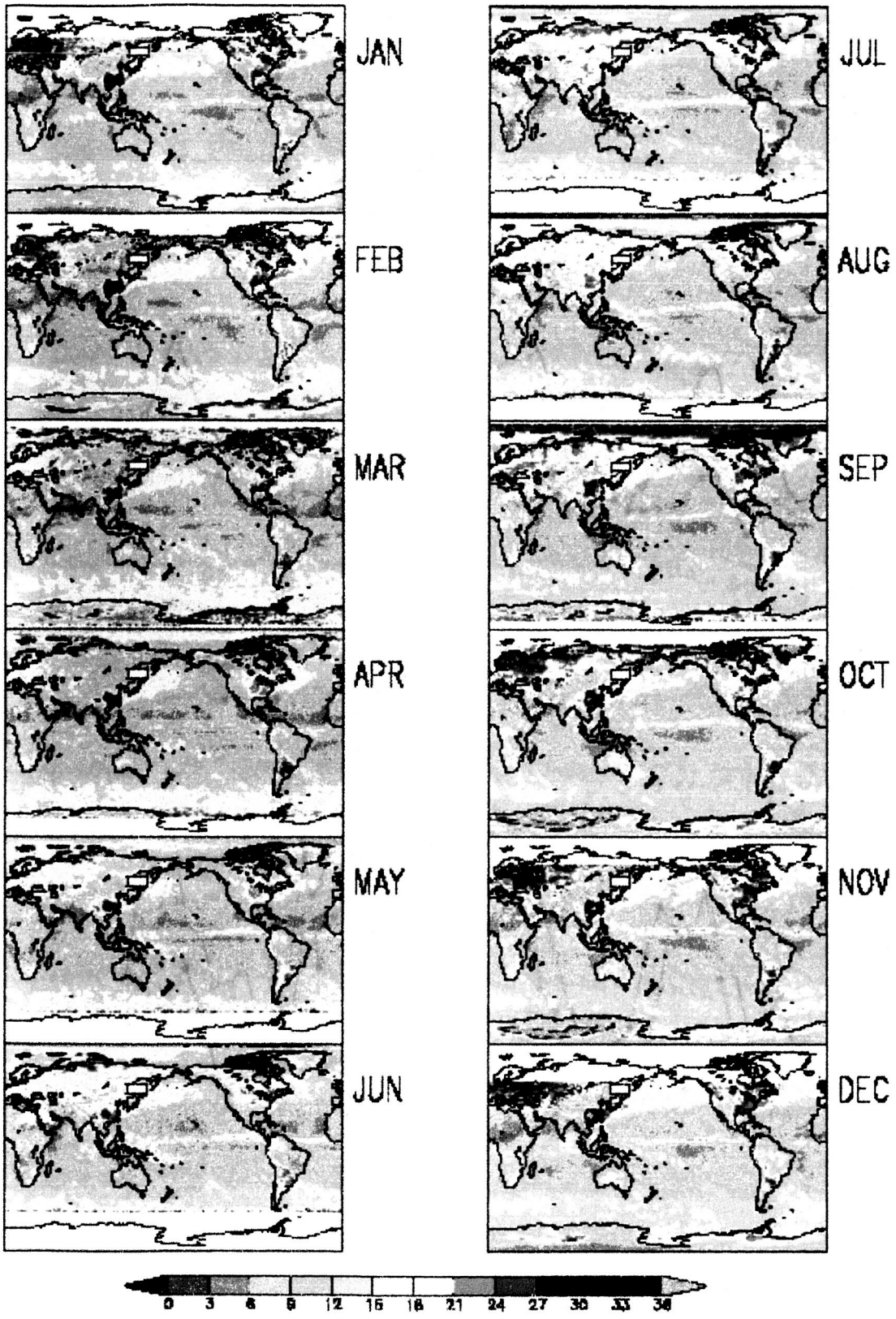

Figure 1. Monthly mean cloud optical thickness from April 2000-July 2003 [should add through March 2004 or 2005 later].

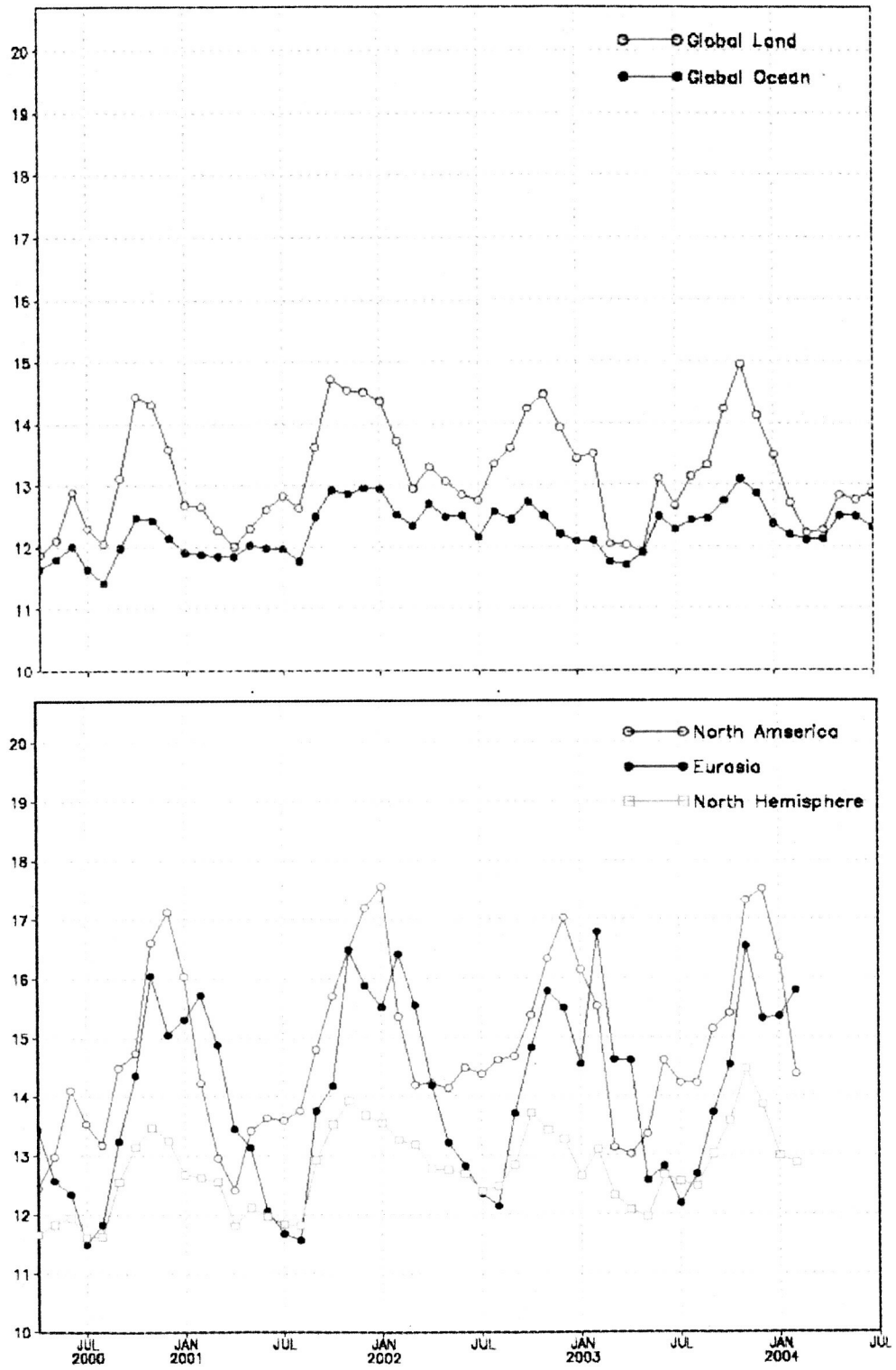

Figure 2. Monthly mean cloud optical thickness as a function of time (a) for global land and ocean, and (b) for North America, Eurasia, and the Northern Hemisphere.

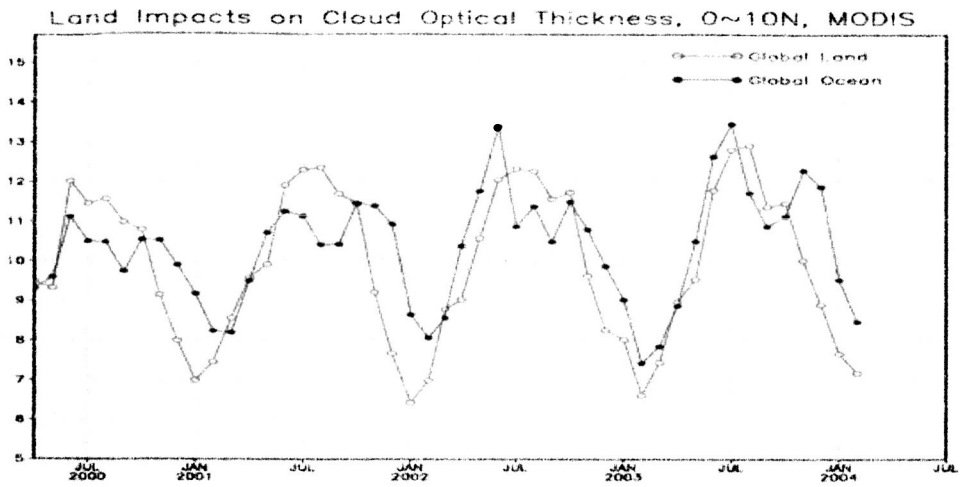
Land Impacts on Cloud Optical Thickness, 0~10N, MODIS
Global Land
Global Ocean
15
14
13
12
11
10
9
8
7
6
5
JUL 2000
JAN 2001
JUL
JAN 2002
JUL
JAN 2003
JUL
JAN 2004
JUL

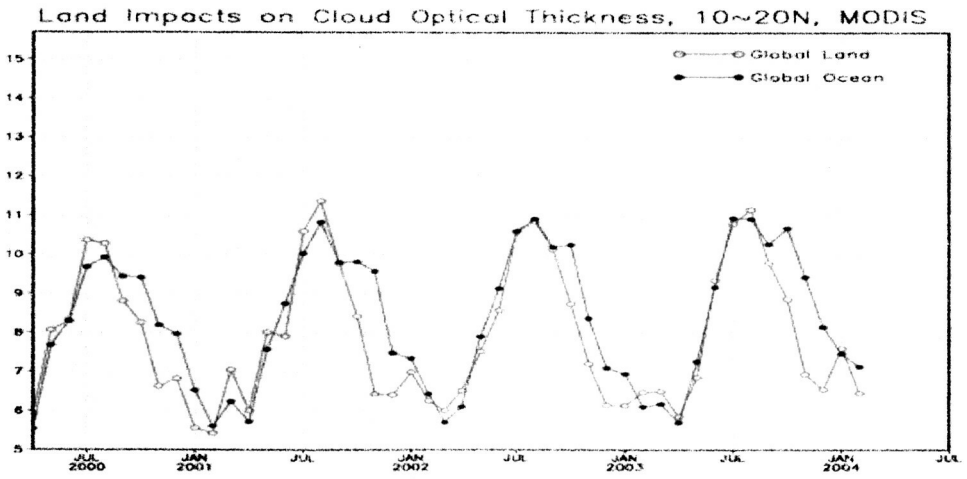
Land Impacts on Cloud Optical Thickness, 10~20N, MODIS
Global Land
Global Ocean
15
14
13
12
11
10
9
8
7
6
5
JUL 2000
JAN 2001
JUL
JAN 2002
JUL
JAN 2003
JUL
JAN 2004
JUL

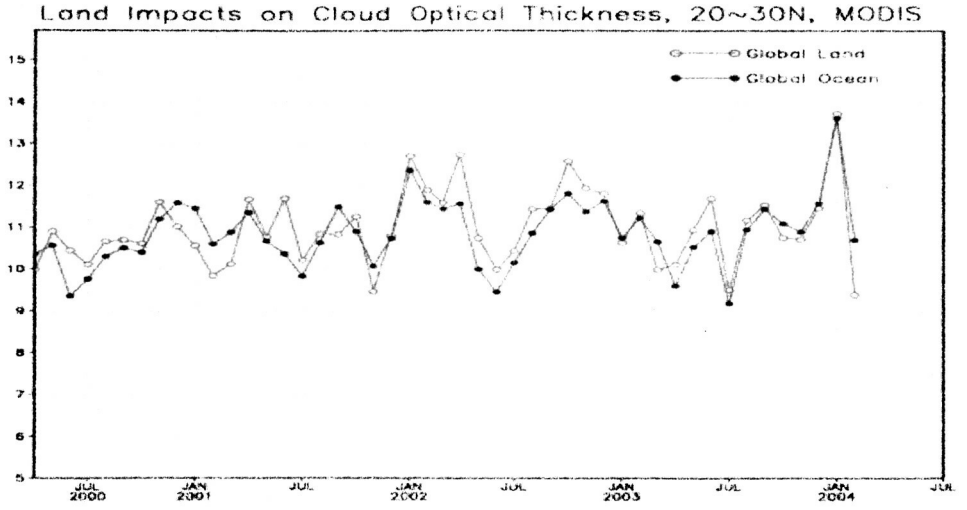
Land Impacts on Cloud Optical Thickness, 20~30N, MODIS
Global Land
Global Ocean
15
14
13
12
11
10
9
8
7
6
5
JUL 2000
JAN 2001
JUL
JAN 2002
JUL
JAN 2003
JUL
JAN 2004
JUL

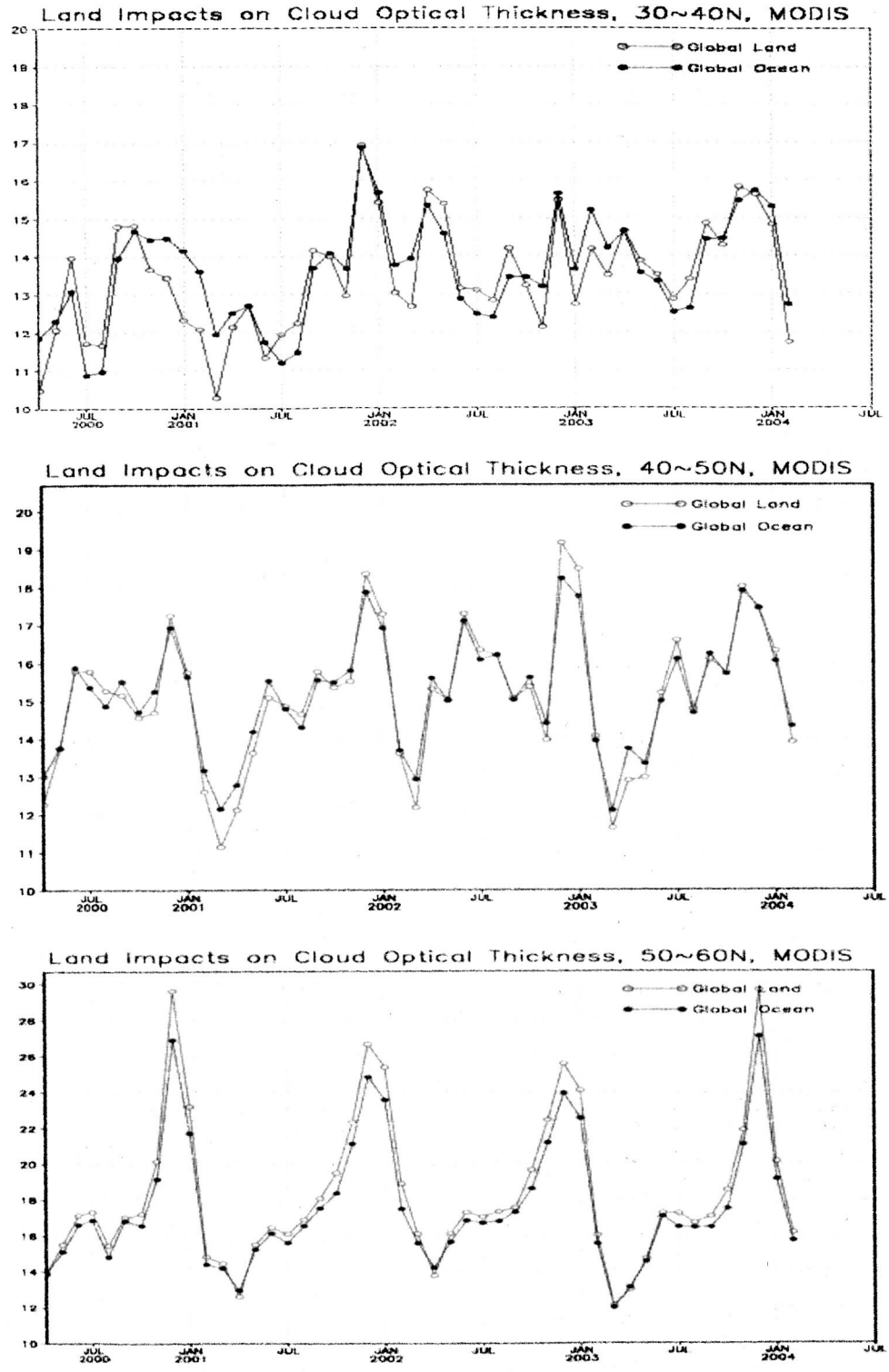

Figure 3. Zonal mean cloud optical thickness as a function of time for land and ocean regimes.

a) Liquid Water Clouds

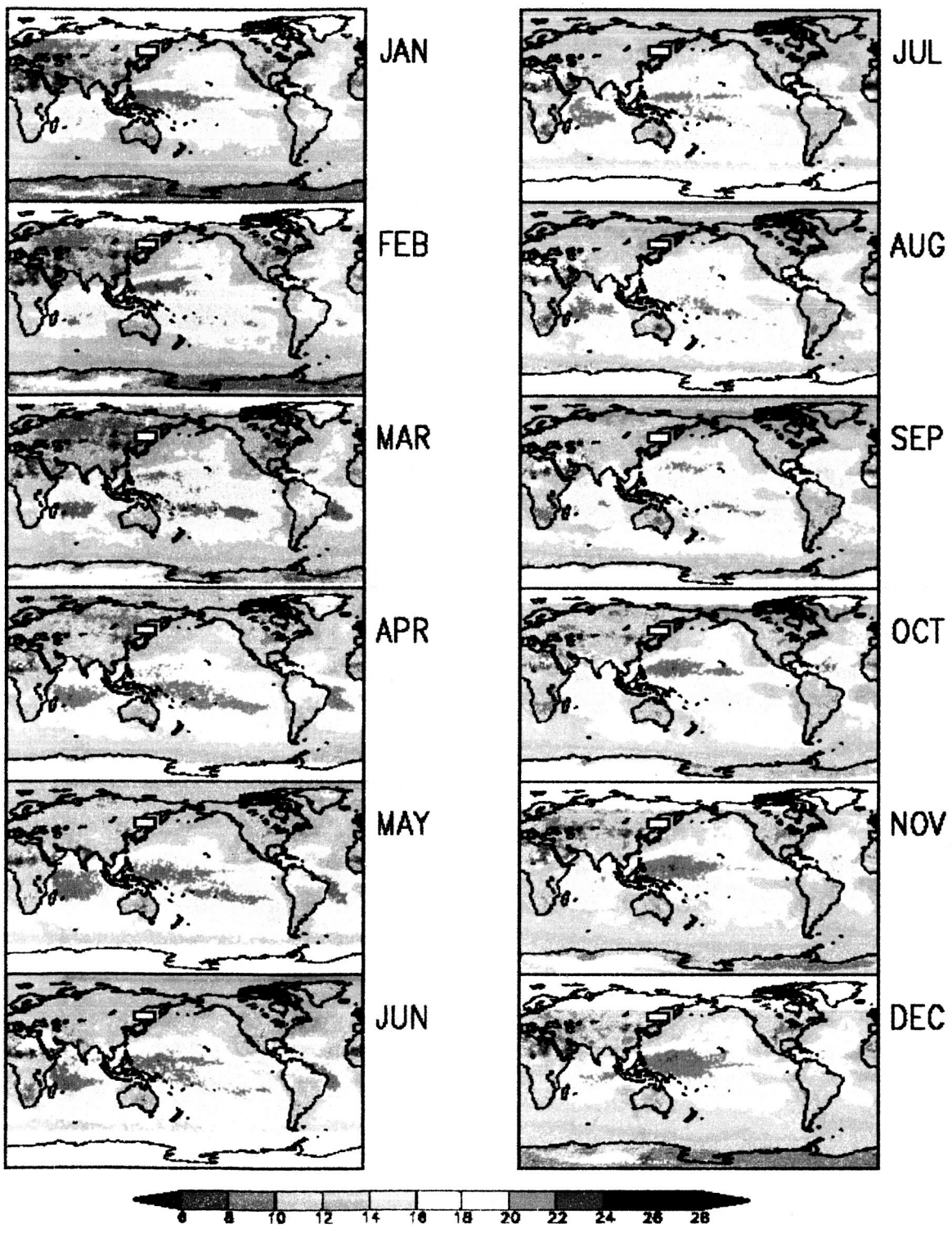

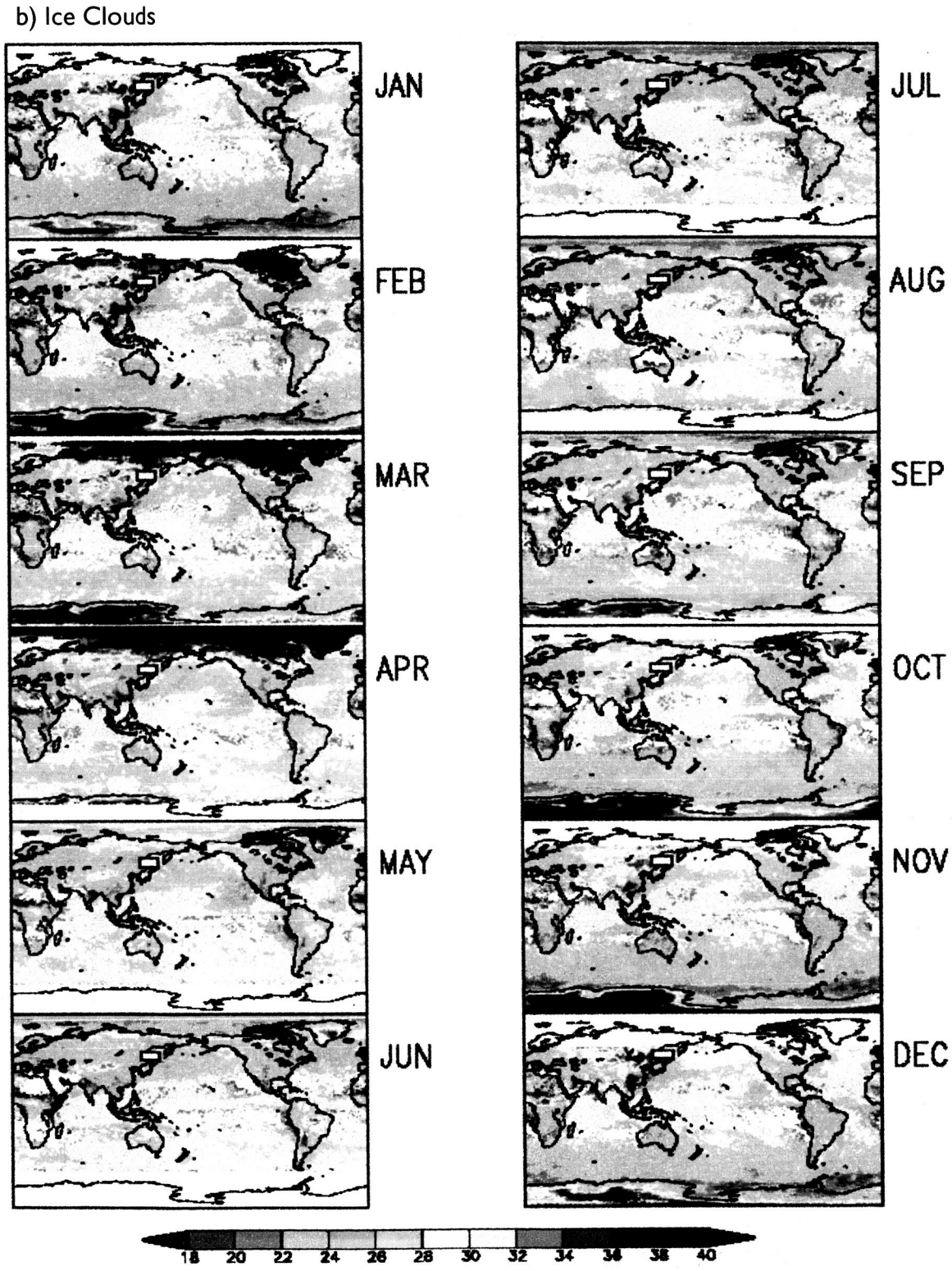

Figure 4. Monthly mean cloud effective radius for (a) liquid water clouds and (b) ice clouds from April 2000-July 2003.

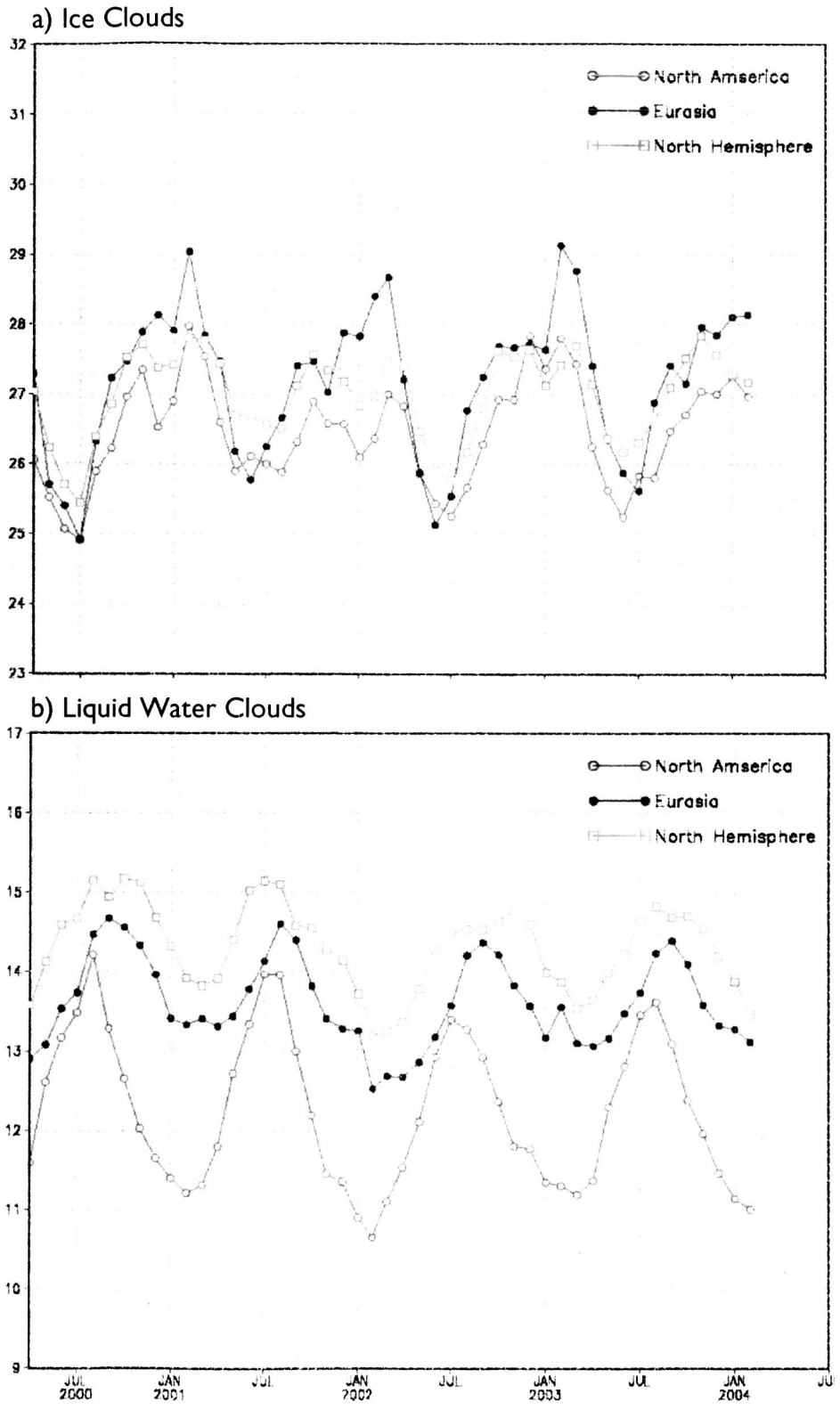

Figure 5. Monthly mean cloud effective radius as a function of time for (a) ice clouds and (b) liquid water clouds.

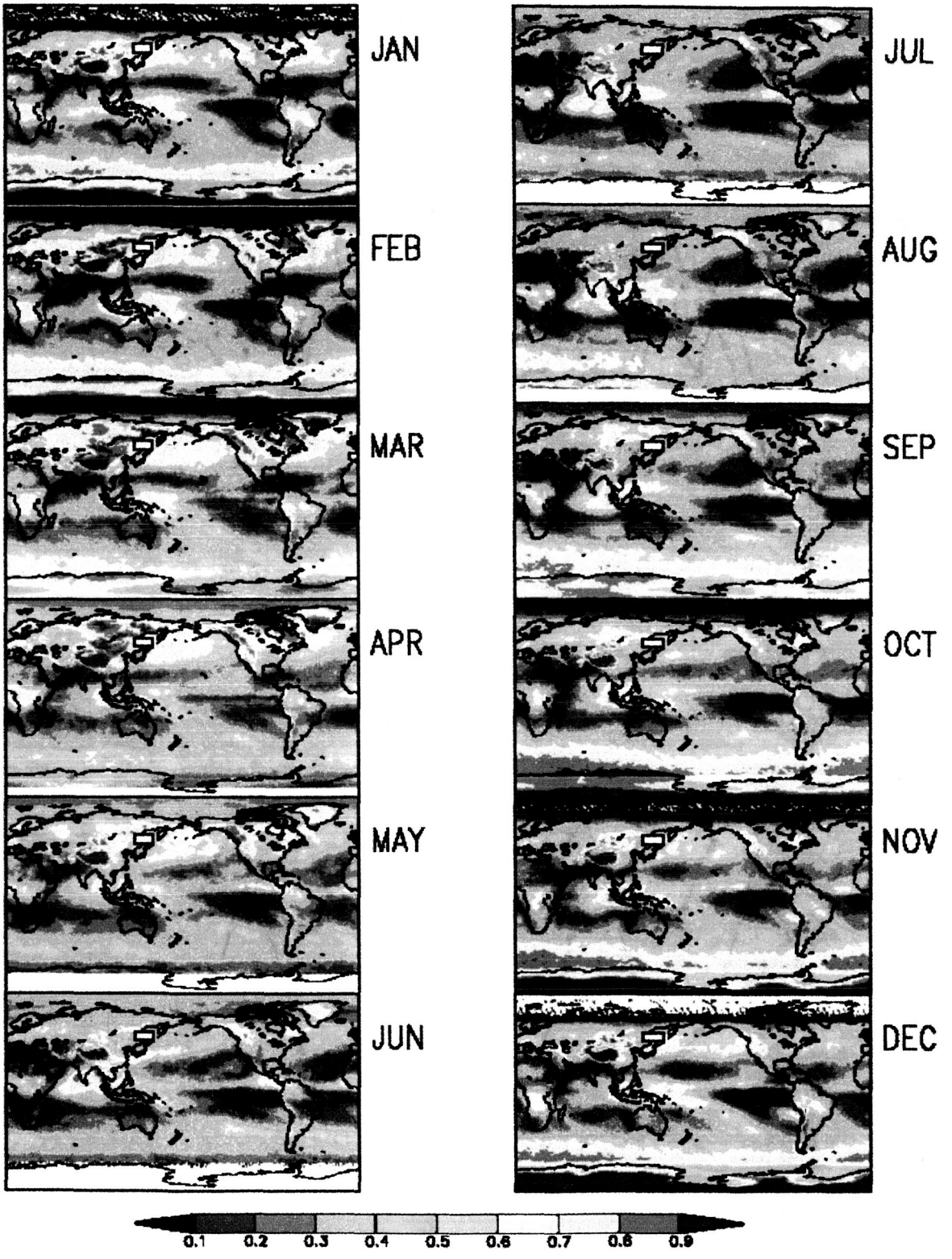

Figure 6. Monthly mean cirrus fraction from April 2000-July 2003.

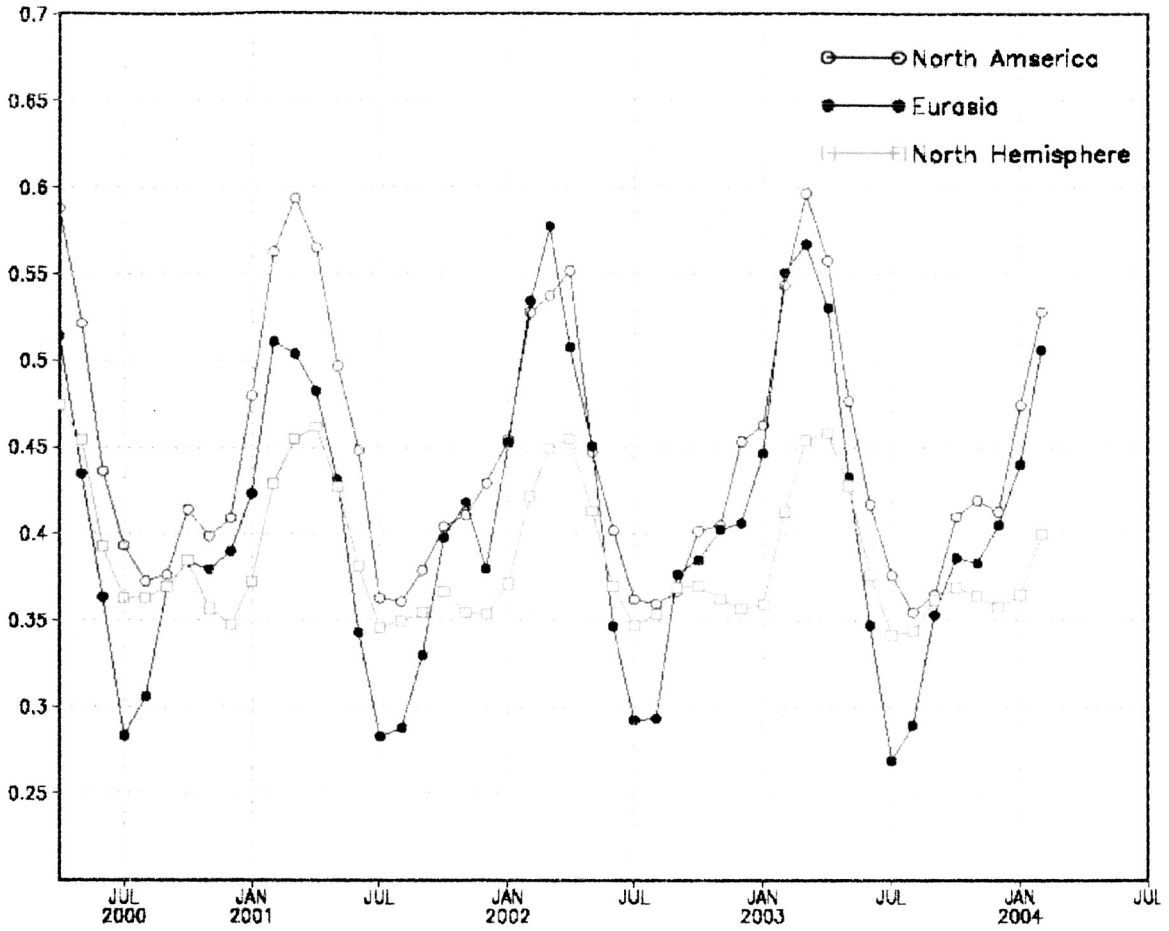

Figure 7. Monthly mean cirrus fraction as a function of time for North America, Eurasia, and the Northern Hemisphere.

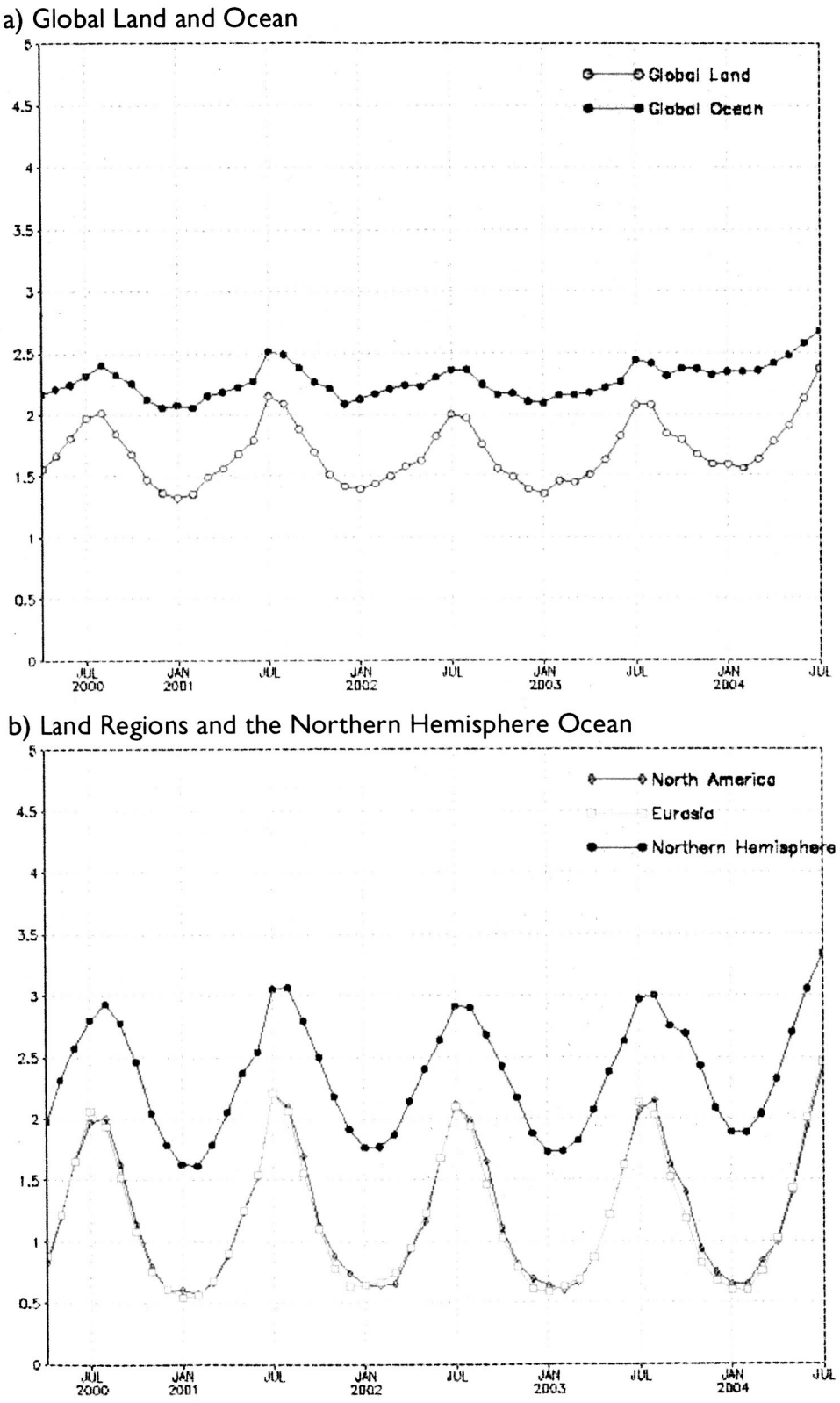

Figure 8: Monthly mean precipitable water as a function of time (a) for global land and ocean, and (b) for North America, Eurasia, and the Northern Hemisphere ocean.

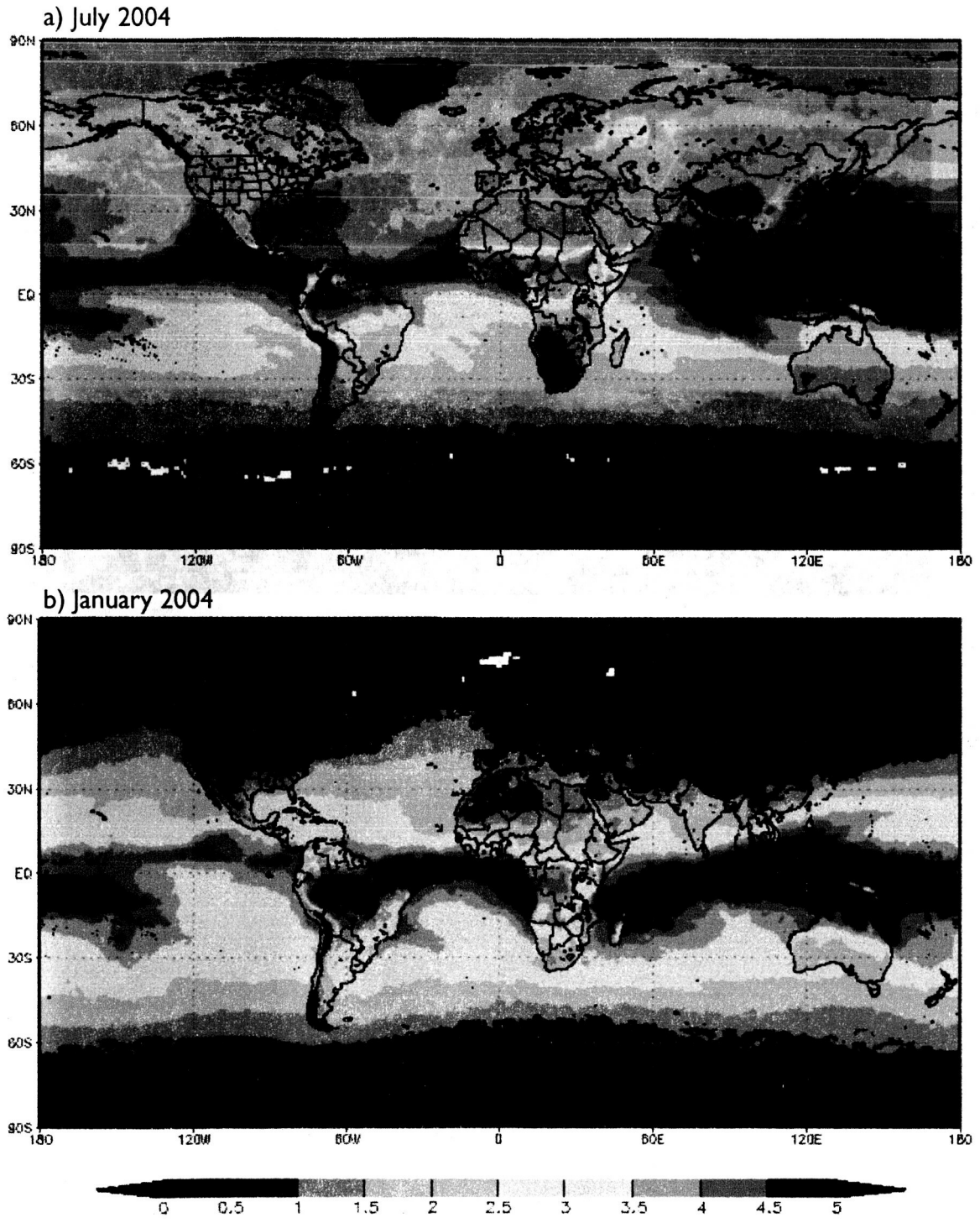

Figure 9: Monthly mean precipitable water for (a) July 2004 and (b) January 2004.

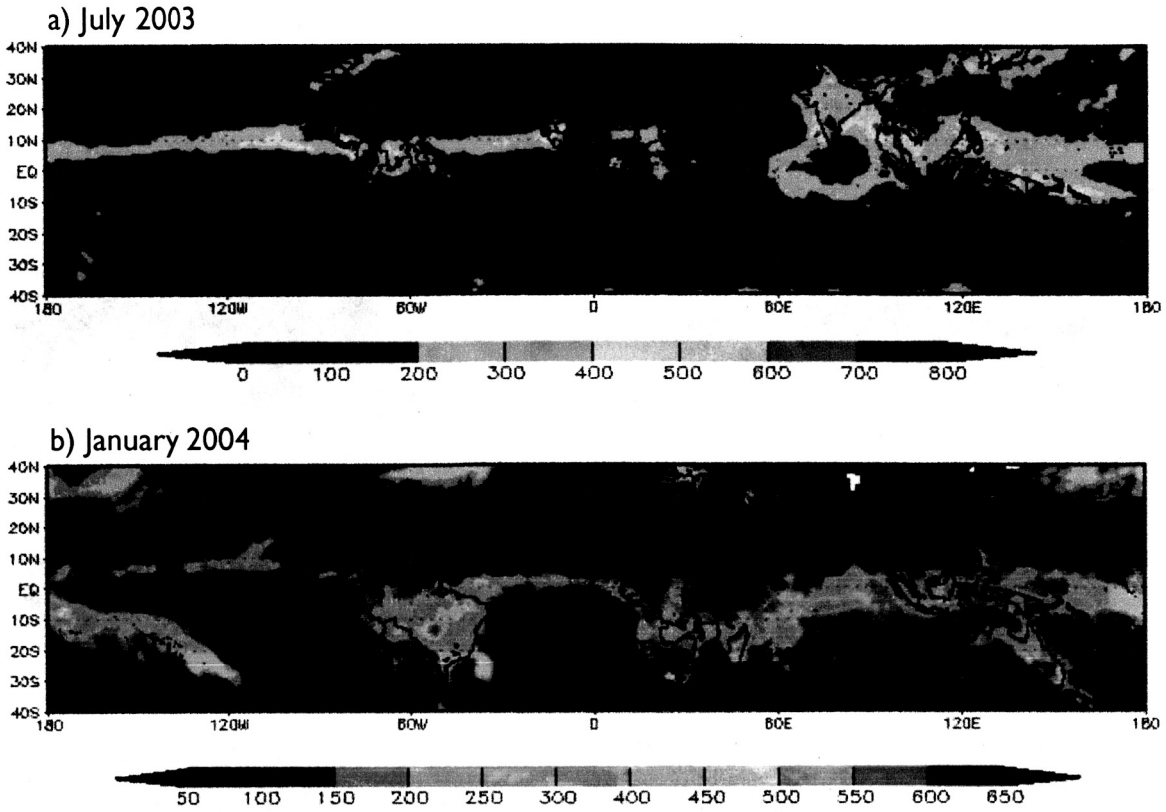

Figure 10. Accumulated rainfall measured from TRMM for (a) July 2003 and (b) January 2004.

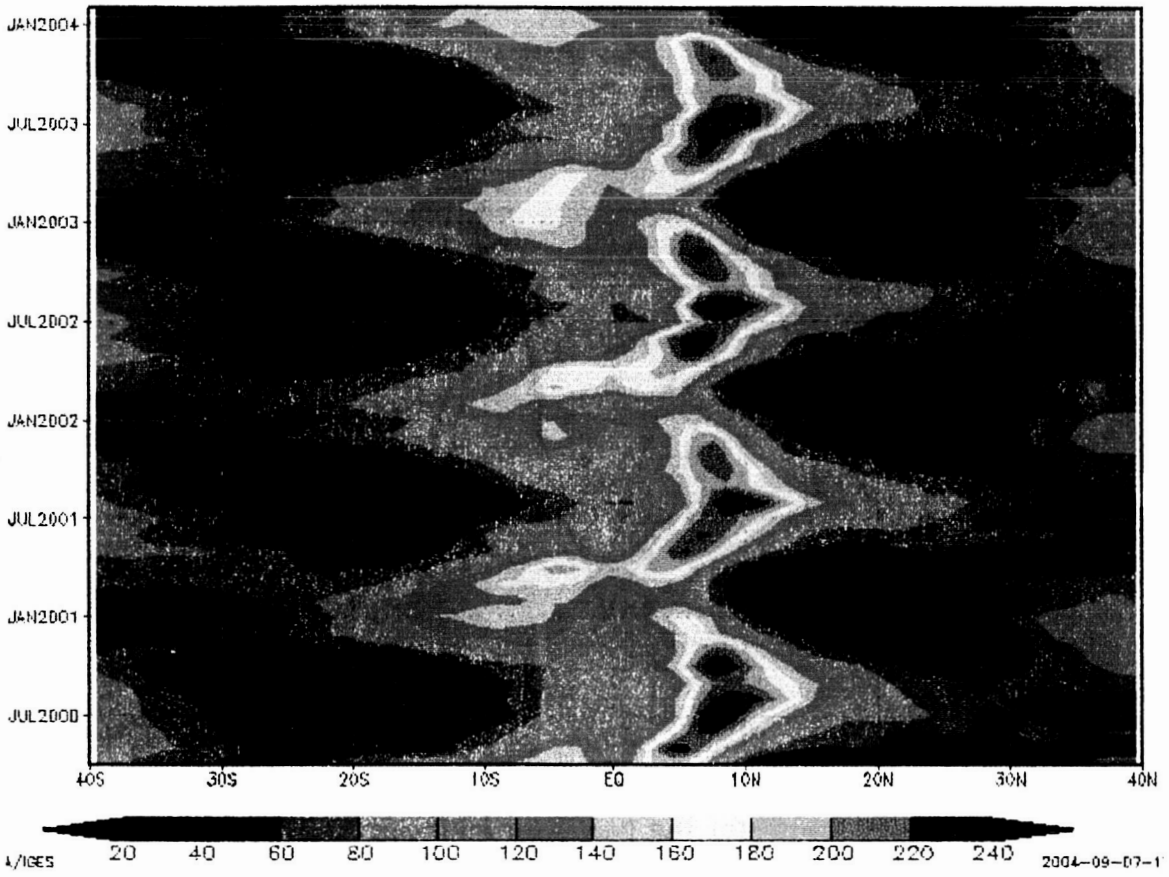

Figure 11. Zonally-averaged monthly mean accumulated rainfall from TRMM observations at 180°W.

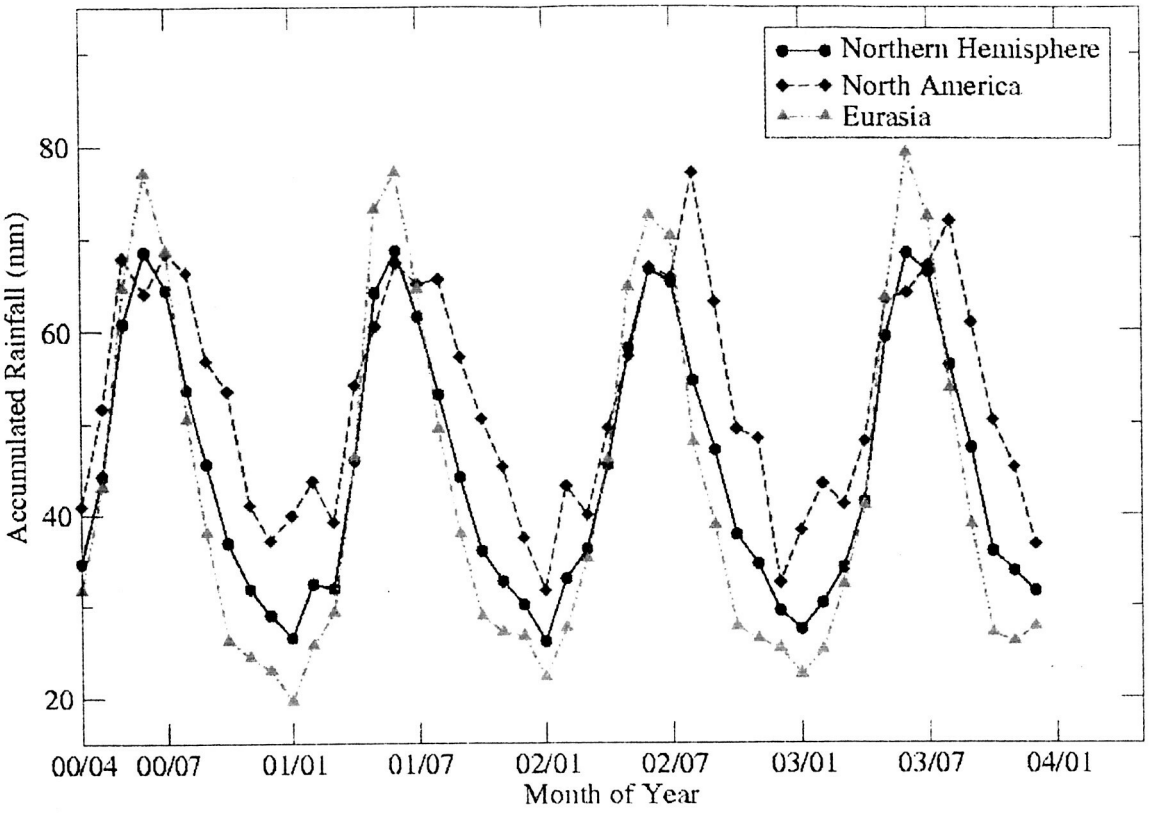

Figure 12. Monthly rainfall for the Northern Hemisphere, North America, and Eurasia. Data are based on GPCP analysis.

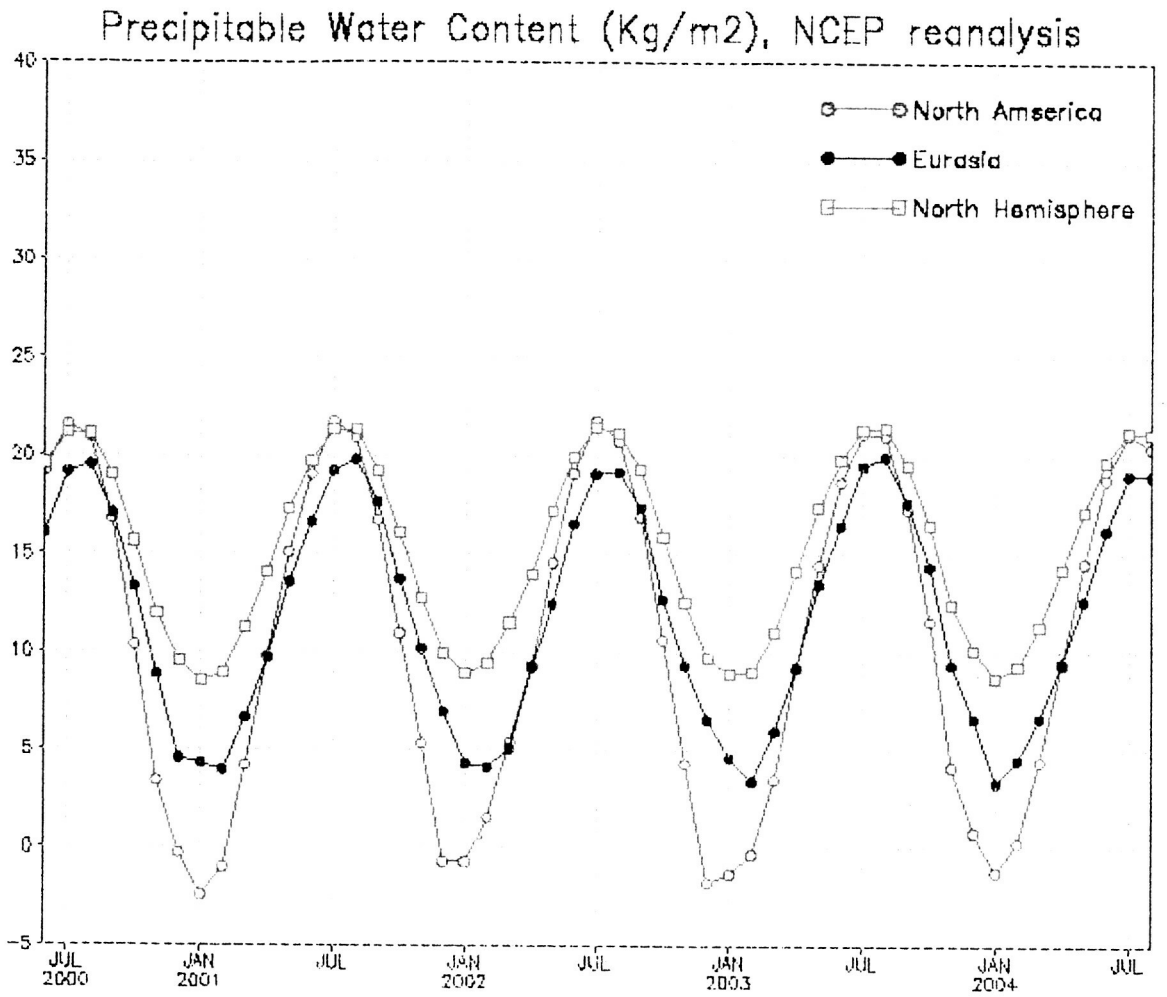

Figure 13. NCEP reanalysis simulated precipitable water vapor for North America, Eurasia, and the North Hemisphere.